Ultramicroscopy 110 (2010) 1435–1442

Contents lists available at ScienceDirect

Ultramicroscopy

journal homepage: www.elsevier.com/locate/ultramic

Single cell mechanics of keratinocyte cells

Valentin Lulevich [a,1], Hsin-ya Yang [b,1], R. Rivkah Isseroff [b,**], Gang-yu Liu [a,*]

[a] Department of Chemistry, University of California, One Shields Ave., Davis, CA 95616, USA
[b] Department of Dermatology, School of Medicine, University of California, Davis, CA 95616, USA

ARTICLE INFO

Article history:
Received 14 February 2010
Received in revised form
5 July 2010
Accepted 27 July 2010

Keywords:
Cell mechanics
Single cell compression
Cytoskeleton
Keratinocyte
Blebbing

ABSTRACT

Keratinocytes represent the major cell type of the uppermost layer of human skin, the epidermis. Using AFM-based single cell compression, the ability of individual keratinocytes to resist external pressure and global rupturing forces is investigated and compared with various cell types. Keratinocytes are found to be 6–70 times stiffer than other cell types, such as white blood, breast epithelial, fibroblast, or neuronal cells, and in contrast to other cell types they retain high mechanic strength even after the cell's death. The absence of membrane rupturing peaks in the force-deformation profiles of keratinocytes and their high stiffness during a second load cycle suggests that their unique mechanical resistance is dictated by the cytoskeleton. A simple analytical model enables the quantification of Young's modulus of keratinocyte cytoskeleton, as high as 120–340 kPa. Selective disruption of the two major cytoskeletal networks, actin filaments and microtubules, does not significantly affect keratinocyte mechanics. F-actin is found to impact cell deformation under pressure. During keratinocyte compression, the plasma membrane stretches to form peripheral blebs. Instead of blebbing, cells with depolymerized F-actin respond to pressure by detaching the plasma membrane from the cytoskeleton underneath. On the other hand, the compression force of keratinocytes expressing a mutated keratin (cell line, KEB-7) is 1.6–2.2 times less than that for the control cell line that has normal keratin networks. Therefore, we infer that the keratin intermediate filament network is responsible for the extremely high keratinocyte stiffness and resilience. This could manifest into the rugged protective nature of the human epidermis.

1. Introduction

Skin is the interface that guards the body interior from external pathogens and is one of its most important protective mechanisms. The uppermost layer of skin, the epidermis, consists primarily of keratinocytes (> 90% of all epidermal cells) [1]. Keratinocytes form an effective barrier to the entry of protein antigens, chemical irritants, and infectious agents into the body [2], all while resisting environment stress, external pressure, and sheer force. Therefore, an understanding of the keratinocyte mechanical properties that underlie these characteristics is critical for optimizing skin integrity and function.

In many cells, the cytoskeletal element that contributes to the skin's physical integrity and ability to withstand various stresses is the actin network. In keratinocytes however, it is the keratin intermediate filament network that is believed to confer mechano-resistive strength to the cell [3]. Indeed, studies in transgenic mice [4] and in patients with heritable fragility of the epidermis [5] have demonstrated that the mechanical strength of epithelial cell sheets is related to the molecular structure of their keratin intermediate filaments (IF) [5]. For example, in human patients with the disease epidermolysis bullosa simplex (EBS), in which the K5 and K14 keratins are mutated, keratinocytes of the basal layer of the epidermis can be easily ruptured and patients develop blisters and erosions of the epidermis [6–8]. Likewise in transgenic mice where the K5 or K14 gene is mutated, a similar blistering and erosive disease of the epidermis ensues [9–12]. Keratin bundles themselves (derived from Hagfish) [13] or even keratin filaments in suspension [14] have unique mechanical properties in terms of elasticity and deformation reversibility. Further, recent work has demonstrated that some keratin molecular species (K6, K16, K17) are expressed uniquely in migrating cells at the edge of a skin wound, and thus are proposed to confer pliability to enhance migratory capacity of keratinocytes needed for wound repair [15]. However, despite the recognized protective roles of the epidermis, systematic, and quantitative investigations on the mechanical resistance of individual keratinocytes in response to external pressure have not been reported.

Atomic force microscopy (AFM)-based single cell compression is a relatively new method introduced in 2006 by our team [16]. This technique enables the establishment of deformation profiles and quantification of the elastic compliance of individual cells.

* Corresponding author. Tel.: +1 530 754 678; fax: +1 530 754 8557.
** Corresponding author.
E-mail address: liu@chem.ucdavis.edu (G.-y. Liu).
[1] Authors contributed equally to this work

0304-3991/$ - see front matter © 2010 Elsevier B.V. All rights reserved.
doi:10.1016/j.ultramic.2010.07.009

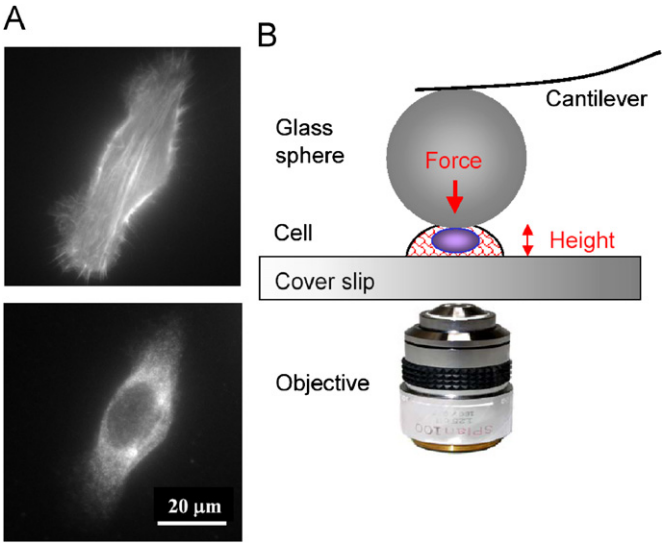

Fig. 1. (A) Epifluorescence microscopy images of a keratinocyte cell containing two immunofluorescent tags: F-actin by phalloidin conjugated to Alexa Fluor 488 (top) and keratin by mouse anti-cytokeratin antibody conjugated with Alexa Fluor 594 (bottom). (B) A schematic diagram illustrates the concept of single cell compression method.

Briefly and as illustrated in Fig. 1, an AFM probe is modified with a large (40–60 μm) microsphere and positioned above the nucleus of a selected cell. When the cell is compressed between the substrate surface and the microsphere, force and cell deformation are recorded using AFM, while optical microscopy monitors the cell shape in real time. Complementary to existing cell mechanics approaches [17], this method capitalizes on the well-known advantages of AFM such as precise probe-cell positioning (10 nm during compression cycle), and direct and accurate deformation measurements to allow a wide force detection range (0.1 nN–50 μN). This technique also provides precise control of the deformation rate (0.1–50 μm/s) at full displacement range, as well as the capability of taking measurements on cells *in vitro*. Due to the large size of the probe, the technique allows measurement of very low values of cellular pressure (up to 10 Pa). In contrast to other methods for measuring cell mechanics, such as magnetic twisting cytometry [18] or AFM force mapping [17], this AFM-based technique does not probe local force or elasticity, but whole-cell's mechanical properties. Full displacement range (0–100% or complete cell compression in most cases) enables investigation of mechanical response of single cells at various deformation states.

Using single cell compression, this investigation focuses on the response of living human keratinocytes under external loading-and-unloading cycles. The force-deformation profiles for the keratinocytes are established, from which the elastic compliance of the membrane and cytoskeleton are extracted. By comparing keratinocytes with other cell types such as white blood, breast epithelial, fibroblast, or neuronal cells, the uniquely strong mechanical resistance of keratinocytes is revealed and quantified. In addition, the cellular components that are responsible for the observed behaviors in these cells are identified.

2. Materials and methods

2.1. Cell preparation

Normal human keratinocytes were isolated from neonatal foreskin, as previously described [19] under an approved exemption granted by the Internal Review Board at the University of California, Davis. Keratinocytes were grown in keratinocyte growth medium (KGM; Epilife, 0.06 mM Ca^{2+}; Cascade Biologics, Portland, OR), supplemented with 1× human keratinocyte growth supplement (Cascade Biologics) and 1× antibiotic–antimycotic solution (Invitrogen, Carlsbad, CA) at 37 °C in a humidified atmosphere of 5% CO_2. Cell culture passages 2–5 were used to assure the fidelity and consistency of these cells. Keratinocyte lines, including the control HPV16 E6/E7-immortalized NEB-1 line and the HPV16 E6/E7-immortalized keratinocyte line KEB-7 expressing mutated keratin 14 (K14), were the kind gifts of Professor Irene Leigh, University of Dundee, UK [8]. NEB-1 and KEB-7 at passage 10–20 were switched from the original DMEM/HamF12 culture medium (3:1 from Invitrogen, supplied with 10% serum, 5 μg/ml transferrin, 0.4 μg/ml hydrocortisone, 10^{-10} M cholera toxin, 10 ng/ml EGF, 5 μg/ml insulin, and 2×10^{-11} M L-iodothyronine) to KGM for compression. Petri dishes with glass bottoms (MatTek, Ashland, MA) were pre-coated with 0.5 mL of 100 μg/ml type I bovine collagen solution (Sigma-Aldrich, St. Louis, MO) for 1 h at 37 °C. Keratinocytes, plated at a final density of 8×10^4 cells/cm^2, were allowed to attach overnight to the collagen pre-coated plates at 37 °C before compression experimentation. Cell compression was performed at room temperature, in the presence of KGM and, in some cases, 0.4% of Trypan blue (Invitrogen, Carlsbad, CA).

To depolymerize F-actin, cells were incubated with 0.2 μg/mL Latrunculin A (Invitrogen, Carlsbad, CA) for 30 min prior to cell compression. For microtubules depolymerization cells were incubated with 10 μM Nocodazole (Sigma-Aldrich, St. Louis, MO) also for 30 min prior to cell compression. Because both Latrunculin A and Nocodazole were pre-dissolved in 100% dimethyl sulfoxide (DMSO, Sigma-Aldrich, St. Louis, MO), control cells for these experiments were also treated with the same concentration of DMSO.

2.2. Immunofluorescence microscopy

Immunofluorescent localization of cytoskeletal elements followed published, standard protocols [20–22]. Briefly, keratinocytes were plated overnight on #1 coverslips (Fischer, Pittsburgh, PA), fixed with 10% buffered formaldehyde (Fisher, Pittsburgh, PA) and blocked with 5% bovine serum albumin (BSA) (Sigma-Aldrich, St. Louis, MO). Keratin was identified using mouse anti-cytokeratin antibody (1:200, Zymed, San Francisco, CA). Anti-cytokeratin antibody was diluted in 5% BSA and incubated with the cells overnight at 4 °C. To label microtubules, mouse anti-beta tubulin I (1:1000, Sigma-Aldrich, St. Louis, MO) conjugated with Alexa Fluor 594 (Invitrogen, Carlsbad, CA) was diluted in 5% BSA and incubated with cells for 2 h at room temperature. Actin filaments (F-actin) were directly detected using phalloidin, an actin-binding toxin isolated from *Amanita phalloidses*, conjugated to Alexa Fluor 488 (1:200, Invitrogen, Carlsbad, CA). Phalloidin was diluted in 5% BSA and incubated with cells for 2 h at room temperature.

Epifluorescent images were captured using a Nikon TE-2000 inverted microscope (Nikon, Melville, NY) with 60× oil objective and a QICAM camera (Qimaging, Surrey, Canada). To image Alexa Fluor 488 and Alexa Fluor 594 dyes, filter sets with maximum excitation/emission 495/519 nm and 590/617 nm were used, respectively. Fig. 1A shows a typical keratinocyte cell stained for F-actin (top), and keratin (bottom).

2.3. Single cell mechanics

Cell deformation was measured with a MFP-3D AFM (Asylum Research Corp., Santa Barbara, CA), which is equipped with a

nanopositioning sensor for monitoring actual piezotranslator motion for correcting piezo hysteresis and creeping. The AFM was combined with an inverted optical microscope IX50 (Olympus America, Center Valley, PA). As schematically shown in Fig. 1B, optical microscopy guides the positioning of the AFM probe to directly above the center of a designated cell (typically the center of nucleus), and allows visualization of the deformation of the cell organelles upon the application of compression force [16]. Cell compression experiments were monitored under bright field illumination to avoid using fluorescent dyes, which have the side effect of stiffening cells [23]. To investigate the cell's mechanical degradation due to compression, multiple loading–unloading cycles were applied. A hard silicon cantilever, AC160 (Olympus America, Center Valley, PA), with a force constant $k=40$ N/m was used in this study. Glass spheres with a diameter of 40 ± 2 μm (Duke Scientific, Fremont, CA) were attached to the apex of the AFM tips using a premixed two-component epoxy glue (Elmer's epoxy resin, Columbus, OH). After sphere attachment, the spring constant was independently calculated according to the added mass method and the results were in good agreement (within 15% for AC240 and 30% for AC160) with values obtained from thermal noise measurements [24,25].

Force-deformation profiles for single cell compression experiments were plotted as loading force versus relative cell deformation. Because cell height can vary from 7 to 13 μm, relative deformation, ε=cell height change/initial cell height, was used to quantify the cell compression. The zero deformation for individual cells was determined from the point of the first detectable force (normally at 1–3 nN level) during the loading cycle. To avoid any significant impact of hydrodynamics, loading and unloading followed a speed of 2 μm/s, well below significant hydrodynamic forces [26]. The load, F, applied to the cell is calculated from Hook's law $F=k\Delta$, where k is the force constant of the sphere-modified AFM cantilever and Δ represents the deformation of the cantilever.

To ensure reproducibility and robustness and to take into consideration cellular heterogeneity, at least 3 independent sets of measurements were performed for each designed experimental condition. In each set, 5–10 healthy cells were chosen to compress. This work reports results from more than 200 control cells in KGM medium, 44 control cells in KGM media containing DMSO, 36 Latrunculin A treated and 22 Nocodazole treated cells, 25 NEB-1 cells and 25 KEB-7 cells. Force and Young's modulus numbers in Table 1 are calculated as average values plus/minus standard deviations. Cells' shape parameters were recorded by video camera for each individual cell, along with data on each cell's size, height, number of blebs, and bleb size.

3. Results and discussion

3.1. Characteristic mechanical properties of keratinocytes

Fig. 1A shows a typical keratinocyte cell upon immobilization on a surface. The cell has a relatively symmetrical shape with a 12 μm nucleus (the dark area) in the center. Immunofluorescent staining was performed to highlight F-actin (Fig.1A, upper panel) and keratin (Fig.1A, lower panel). High-density keratin filament networks are homogeneously distributed in the cytosol, while actin filaments are mostly concentrated at the membrane periphery. Among keratinocytes imaged, the lateral dimensions range 35–55 μm and typical height is 10 ± 3 μm, as measured by AFM at the central point above nucleus and the glass substrate. The geometry measured here correspond well with published investigations [27].

Fig. 2A shows a typical force profile of a keratinocyte, and Fig. 2B and B′ are two optical micrographs serving as examples of the keratinocyte's deformation and bleb due to compression. The single cell compression method allows the recording of both the loading, which contains information about cell mechanical resistance, and unloading part of the curve, which reveals cell-probe adhesion. Only the loading cycle of the force-deformation profile is discussed in this article to maintain scientific focus. The keratinocyte has a smooth deformation profile without irregularities or stress peaks, in contrast to that of T cells [16]. Typical force is 0.4 ± 0.1 μN to reach 30% compression, and 6.0 ± 2.0 μN at 80% of its original height (see also Table 1, row 1). When deformation exceeds 50%, the cell develops 2–8 membrane extrusions, or blebs, 4–16 μm in diameter, indicated in Fig. 2 by red arrows. Upon unloading, the blebs partially retreat, but do not completely disappear, as indicated in Fig. 2B, middle row. Such blebs are similar to the blebs occurring during apoptosis or cytokinesis [28,29], and represent detachment of the plasma membrane from the cytoskeleton due to an increase in intracellular pressure driven by the external load. A simultaneous Trypan blue assay [30] suggests that the membrane becomes permeable beyond 10 ± 3 μN. After this threshold load, cells remained blue for the duration of the experiments, for example, from 20 to 30 min, and therefore membrane healing did not occur. Because the typical keratinocytes remain viable at small deformation, but bleb and die at high force, we provide two force values in Table 1, at $\varepsilon=0.3$ (living cells) and $\varepsilon=0.8$ (dead cells), to characterize the two states.

The second deformation profile allows us to measure the cell's degradation due to the first cycle [16]. The keratinocyte exhibits a smooth profile in the second cycle, and more importantly, the cell

Table 1
Comparison of single cell mechanics of keratinocytes to cell lines derived from different organs (all profiles were acquired during the first cycle unless specified).

Index	Cell type (organ)	F (μN) at $\varepsilon=0.3$	F (μN) at $\varepsilon=0.8$	Cell shape at high ε	E_m (MPa)	E_c (kPa)
1	Normal Human Keratinocyte (NHK) primary culture, first cycle (foreskin)	0.4 ± 0.1	5.5 ± 1.5	3–10 blebs	39.5 ± 7.5	290 ± 170
2	NHK, second cycle	0.2 ± 0.1	2 ± 0.9	3–10 blebs	N/A	182 ± 58
3	NHK, DMSO treated	0.35 ± 0.05	5.5 ± 1.5	3–9 blebs	18–22	243 ± 37
4	NHK, Latrunculin A treated	0.3 ± 0.05	4.5 ± 1.5	Membrane detaching from cytoskeleton	21.5 ± 11	112 ± 31
5	NHK, Nocodazole treated	0.33 ± 0.13	5.5 ± 1.5	4–11 blebs	29.5 ± 3	166 ± 12
6	Keratinocyte, NEB-1 cell line	0.13 ± 0.04	2.1 ± 0.7	5–12 blebs	8 ± 2	24 ± 7
7	Keratinocyte, KEB-7 cell line	0.06 ± 0.03	1.3 ± 0.3	6–10 blebs	3 ± 2	20 ± 8
8	Jurkat T cell [16] (blood)	0.06 ± 0.03	0.2 ± 0.1	Membrane bursting, no blebs	20 ± 10	4.5 ± 1.5
9	MDA-MB-468 [23] (epithelial cells, breast cancer)	0.095 ± 0.055	0.45 ± 0.15	4–11 blebs	2.3 ± 0.8	15 ± 6
10	MLC-SV40 [23] (epithelial cells, prostate cancer)	0.045 ± 0.015	0.47 ± 0.15	5–10 blebs	3.3 ± 1.6	19.5 ± 6.5
11	N2a [34] (neuronal tumor)	0.0068 ± 0.0028	0.235 ± 0.045	3–8 blebs	0.9 ± 0.4	N/a

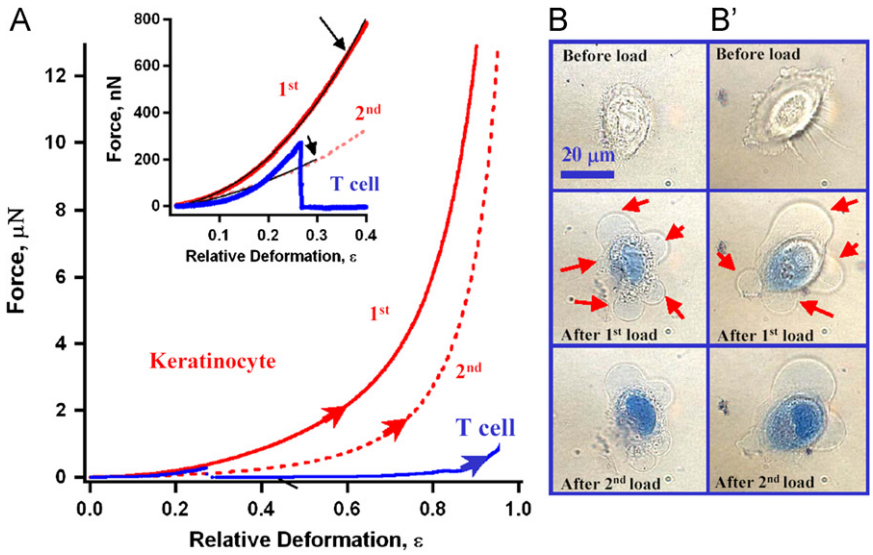

Fig. 2. (A) Force versus relative deformation profile for a typical keratinocyte cell (red) Curves 1 and 2 correspond to the first and second loading cycles. Deformation profile for a typical Jurkat T cell is shown in blue as a comparison. Results from the least square fitting of the deformation profiles, using Eqs. (1) and (2), are shown in the inset (black lines indicated by black arrows). (B) and (B′) represent optical microscopy snapshots of two typical keratinocytes. From top to bottom are: cells before, after the first cycle, and after the second compression, respectively. Force-induced blebs are indicated by the red arrows. Blue color reflects Trypan blue staining after cell membrane became permeable. (For interpretation of the references to colour in this figure legend, the reader is referred to the web version of this article).

returns to its original height. Considering the first cycle involved 90% deformation, the keratinocyte's behavior is in sharp contrast to T or epithelial cells that barely show any elasticity during the second loading. Specifically, for the cell shown in Fig. 2, the initial height measured 7.82 ± 0.05 μm and became 7.76 ± 0.05 μm after the first cycle with the highest load of 50 μN. In the second cycle, the keratinocyte retained mechanical resistance, as can be seen from the similarity between the first and second profiles shown in Fig. 2. For instance, in the second cycle, it required 0.2 ± 0.1 μN to deform the cell to 30% of its original height, and 2.0 ± 1.0 μN of force for 80% deformation, only 2–3 times less than that for the first load (the corresponding force during the first cycle is 0.4 ± 0.1 and 6.0 ± 2.0 μN, respectively). From the optical microscopy, neither additional blebs nor significant changes in cellular morphology evolution were observed in comparison with the first cycle (see Fig. 2B–B′, bottom row).

Unique among all cell types investigated so far, even though the cell membrane is no longer intact, and the cell is no longer viable due to high forces applied in the first cycle, keratinocytes retain significant mechanical resistance. Regardless of the viability of keratinocytes, the mechanical resistance measured is much higher than that of other cell types.

3.2. *Quantification of Young's modulus of the cellular membrane and cytoskeleton*

The results from single cell compression reveal that keratinocytes are much stiffer than many other cell types. Quantitative analysis of keratinocyte force profiles becomes necessary to understand the contributions by the membrane and cytoskeleton components of the cell. While numerical methods as Finite Element Analysis (FEA) would be an ideal match to quantify our data completely, this initial investigation shows a simpler means to quantify only Young's modulus so that important physical insights may be extracted quickly from the measurements.

Derived from the elastic theory of membranes [31] and Hertzian contact mechanics [23,31], our simple analytical model is valid only at small deformations of the living cell (that is, when ignoring membrane's permeability). This approach enables membrane and cytoskeleton contribution to be extracted separately from the force-deformation profile, via a simple analytical expression. Briefly, this model assumes: (a) the single cell compression process may be treated as a spherical membrane filled with an incompressible fluid (balloon) pressed between the parallel plates; (b) at small deformations, the membrane (shell of balloon) is impermeable; (c) a cell's mechanical resistance arises from membrane stretching and cytoskeletal deformation with negligible contributions from other cellular components such as the nucleus at small deformations [32]. For elastic deformation regimes the keratinocyte mechanical resistance can be estimated as:

$$F = F_{\text{cytoskeleton}} + F_{\text{membrane}} = \frac{\sqrt{2}E_c}{3(1-\nu_c^2)} R_0^2 \varepsilon^{3/2} + 2\pi \frac{E_m}{1-\nu_m} h R_0 \varepsilon^3 \qquad (1)$$

where ε is relative deformation of the cell, R_0 and h are the radius of the uncompressed cell and its membrane thickness, and E_m and ν_m represent Young's modulus of the membrane; and E_c and ν_c represent Young's modulus and the Poisson ratio of the cytoskeleton, respectively. The physical meaning of Eq.(1) indicates that the mechanical resistance of a single cell arising from cytoskeletal compression follows the $F \propto E_c \varepsilon^{3/2}$ relationship; and a $F \propto E_m \varepsilon^3$ term from the membrane stretching. The fact that the deformation profile for the membrane and cytoskeleton follows different power laws (3 versus 3/2) allows us to extract both E_m and E_c from the same cell compression profile using one non-linear fitting step.

Fitting individual deformation profiles using Eq. (1) in the deformation range 0–30% enables single cell elasticity to be quantified. The quality of the fitting can be examined by comparison of the data versus the model as shown in Fig. 2, as well as by the relatively low χ^2 (chi-square) values, ranging from 8×10^{-15} to 2×10^{-14}. For the cell shown in Fig. 2, the E_m and E_c are 31.2 ± 0.13 MPa and 339 ± 7 kPa, respectively ($\chi^2 = 3.9 \times 10^{-14}$). Other parameters include: membrane thickness $h = 4$ nm [16], $R_0 = 3.7$ μm, that is, 1/2 of cell height, $\nu_m = 1/2$ for the cell membrane (i.e., incompressible), and $\nu_c = 0$ (fully compressible).

Note that the v value of cytoskeleton contribution depends on membrane–cytoskeleton interactions. For a detached cytoskeleton, our assumption $v=0$ is accurate. For a strongly attached membrane, lateral cytoskeleton extension may occur during compression, which would result in higher effective v_c, between 0 and 0.5. A much more complex model is needed to account for such a cytoskeleton extension. However, due to the mathematical expression, $1/(1-v^2)$, derived from the Hertzian model, even $v=0.25$ would only impact the calculation by 6%, which is insignificant. Thus we proceed with $v=0$, in this initial effort to quantify the force profile.

Results for Young's modulus calculated for the keratinocyte membrane and cytoskeleton are summarized in Table 1. Young's modulus of the keratinocyte membrane ranges 23–38 MPa, similar to that of T cells (10–30 Mpa), however, Young's modulus for the keratinocyte cytoskeleton is 120–340 kPa, 25–30 times higher that of T cells (see also Table 1 rows 1 and 8). These results suggest that the keratinocytes' high elastic compliance arises mainly from the cytoskeleton. Young's modulus of the keratinocyte cytoskeleton is only 2–4 times smaller than Young's modulus derived for macroscopic human skin [33], which ranges from 420 to 850 kPa.

After the first compression, the cell membrane became permeable, as indicated by the Trypan blue assay (Fig. 2, bottom row of B and B′). Therefore, for the second compression the membrane stretching term in Eq. (1) can be neglected. The force-deformation follows a simple one-term relationship in Eq. (2) during the second compression cycle:

$$F=\frac{\sqrt{2}E_c}{3(1-v_c^2)}R_0^2\varepsilon^{3/2} \quad (2)$$

Fitting to the second loading curve in deformation range 0–30% is shown in the Fig. 2 inset, with Young's modulus of the cytoskeleton of 228 ± 5 kPa. For typical keratinocytes examined, Young's modulus ranges from 124 to 240 kPa, as summarized in Table 1, row 3. The fact that E_c from the second compression is just 30% less than that for the first cycle, not only reveals a low degree of mechanical degradation in the keratinocyte cytoskeleton, but also validates our model. The high elastic compliance as well as the little degradation of cytoskeleton is unique to keratinocytes, in contrast to T-lymphocyte, breast epithelial, neuronal tumor, and fibroblast cells, which exhibit much softer force profiles in the first cycle and little mechanical resistance during second compression [16,23,34].

3.3. Contribution of cytoskeleton networks to the observed keratinocyte mechanics

Typically the cytoskeleton of eukaryotic cells is composed of three filamentous networks: actin filaments (F-actin), microtubules and intermediate filaments (IF) [3]. Therefore, by sequentially disrupting one of these three cytoskeletal networks, we hope to reveal individual contributions to the keratinocyte's unique mechanics.

F-actin is concentrated just beneath plasma membrane and is the major cytoskeletal component of lamellipodia and filopodia [30]. F-actin is tightly linked with the plasma membrane and plays a key role in cell motility [30]. It has also been shown that actin filaments contribute to cell mechanical resistance [35] and blebbing [28,29].

Microtubules are present as composites in various cellular structures, including the mitotic spindles of dividing cells, and form the tracks for vesicular transport [30]. Microtubules are also believed to be stiff enough to provide the cell mechanical support and determine cell shape [30].

Keratins form the major IF network in epithelial cells, including keratinocytes. Keratin filaments are heteropolymers composed of a paired acidic (type I) and basic or neutral (type II) keratin [4]. In the keratinocytes of the less-differentiated basal layer of the epidermis, the type II keratin 5(K5) is paired with type I keratin 14 (K14), while in the more differentiated upper layer of the epidermis the keratinocytes express the K1/K10 pair instead. There are no chemicals to disassemble keratin filaments in living cells [2]. Therefore, we used the K14 mutant KEB-7 cell line, which was derived from a patient with the Dowling–Meara subtype of severe EBS, in which keratinocytes carry a CGC→CCC mutation in codon 125 of the HKRT14 gene that results in a R125P amino acid alteration in the K14 protein sequence [8]. These cells have abnormal keratin filaments and exhibit keratin network collapse. Thus, they were a good candidate to examine the contribution of an intact keratin network to cell compressibility.

We note that the contribution of the nucleus is excluded from our discussion because it is insignificant based on prior AFM and micropipette aspiration studies [32]. Young's modulus of nuclei fell in the range 1–5 kPa, which is 20–200 times below Young's modulus estimated for the keratinocyte cytoskeleton. The plasma membrane is not mainly responsible for observed high keratinocyte stiffness, because cells retain high stiffness (Fig. 2 and pertaining discussions above) even after membrane become permeable.

3.3.1. Contribution of F-actin

In order to study the role of actin filaments in the context of keratinocyte mechanics, cells were treated with Latrunculin A, a drug that specifically disrupts F-actin by binding to monomeric G-actin to inhibit F-actin assembly without impacting cell viability or interfering with either microtubules or IF filaments [36–38]. A typical epifluorescence image of a normal, control cultured keratinocyte (Fig. 3B) shows distinctive filamentous organization of phalloidin-labeled actin (green filaments), which disassembles in cells treated with Latrunculin A (Fig. 3C).

Deformation profiles for control untreated, compared with Latrunculin A-treated keratinocytes, are shown in Fig. 3A. Smooth force profiles for Latrunculin A-treated cells appear to be slightly below that for control (DMSO-treated) cells. Force in the range of 4–7 μN is required to deform control cells to 80% of their original height, in comparison to 3–6 μN for Latrunculin A-treated cells (see Table 1, row 3 and 4). Fitting the deformation profiles using Eq. (1) yields the E_m values of Latrunculin A-treated cells, 11–32 MPa, almost identical to the control. However, Latrunculin A-treated cells do reveal a softer cytoskeleton, 1.8–2.5 times smaller in E_c, than untreated cells (see Table 1, rows 3 and 4). Thus the contribution of F-actin according to our measurements: weakening Young's modulus for the cytoskeleton by approximately 50%.

Optical monitoring of the deformation process reveals a significant difference between treated and untreated cells. In contrast to control cells that bleb under compression, Latrunculin A-treated cells did not bleb, instead exhibiting almost complete membrane detachment from cytoskeleton. As one can see from Fig. 3E, the membrane of a compressed Latrunculin A-treated cell formed a large bubble. The clearly resolved boundaries of the membrane and cytoskeleton indicate that the bubble represents the detached membrane. This behavior, upon depleting F-actin, supports the notion that F-actin anchors plasma membrane to the rest of the cytoskeleton.

3.3.2. Contribution of microtubules

Nocodazole is able to reversibly depolymerize the microtubule component of the cytoskeleton without interfering with F-actin or

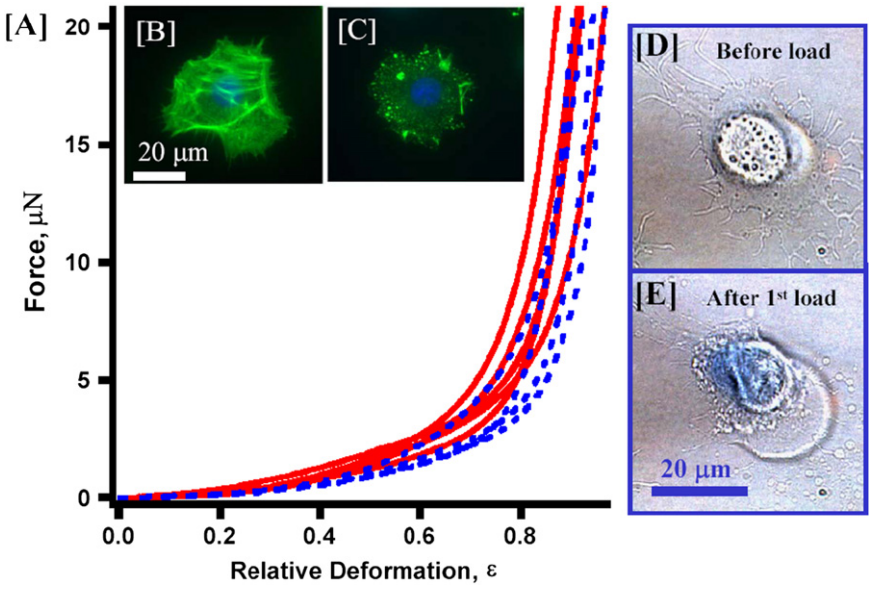

Fig. 3. (A) Characteristic force versus relative deformation profiles for keratinocyte cells treated with Latrunculin A (blue, dashed) in comparison with control (red, solid) (B) and (C) are epifluorescence microscopy images of a control and a Latrunculin A-treated keratinocyte, both subject to philoidin assay to reveal F-actin network. Optical images are of a Latrunculin A-treated keratinocyte before (D) and after (E) compression, where plasma membrane detachment from the cytoskeleton is clearly visible in (E). (For interpretation of the references to colour in this figure legend, the reader is referred to the web version of this article).

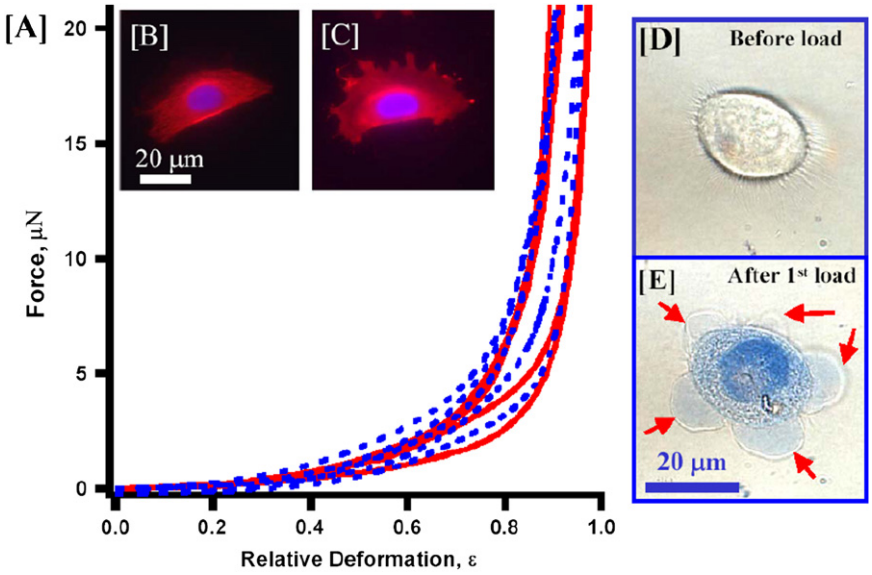

Fig. 4. (A) Characteristic force versus relative deformation profiles for Nocodazole-treated keratinocyte cells (blue, dashed) and control (red, solid) (B) and (C) are epifluorescent images of control and Nocodazole-treated keratinocyte cells containing mouse anti-beta tubulin to reveal microtubules (red). Optical images are of a Nocodazole-treated keratinocyte cell before (D) and after (E) compression, where blebbing occurred due to loading (as indicated by red arrows). (For interpretation of the references to colour in this figure legend, the reader is referred to the web version of this article).

IF filaments [39,40]. Typical epifluorescence images of control, untreated keratinocytes (Fig. 4B) shows the distinctive filamentous organization of microtubules (red filaments), which disappears in Nocodazole-treated cells (Fig. 4C). However, despite the perinuclear collapse of the microtubule network, as shown in Fig. 4C, Nocodazole-treated keratinocytes maintain a normal crescent shaped morphology.

Deformation profiles for control and Nocodazole-treated keratinocytes are shown in Fig. 4A. No significant difference was detected due to the Nocodazole treatment. Force in the range of 4–7 μN is required to deform control cells to 80% of their original height, in comparison with the 3–7 μN for Nocodazole treated cells (see Table 1, rows 3 and 5). Fitting the deformation profiles using Eq. (1) yields the E_m values of Nocodazole -treated cells, 27–32 MPa, almost identical to the control. Latrunculin A-treated cells do reveal a softer cytoskeleton, 1.3–1.5 times smaller in E_c than untreated cells (see Table 1, rows 3 and 5).

Optical monitoring of the cell shape (Fig. 4D and E) during compression shows very similar behavior in both treated and control cells: Nocodazole-treated cells develop 3–7 blebs with the diameter of 3–13 μm. Taking optical monitoring collectively with force profiles, we conclude that microtubules do not play a significant role in the observed keratinocyte mechanics.

3.3.3. *Contribution of keratins*

To further study the contribution of keratin filaments to keratinocyte stiffness, we performed compression with a K14

mutant cell line. Since immortalization with viral proteins, such as HPV16 E6/E7, used to immortalize the KEB-7 line, can lead to unpredictable protein expression changes within the target cells, we used the similarly HPV16 E6/E7-immortalized NEB-1 cell line as a control to avoid potential changes of physical properties of keratinocytes introduced by immortalization. Both cell lines chosen for this study are morphologically identical to primary keratinocytes, and had lateral dimension at the surface of 25–35 μm. Typical height of non-compressed cells measured by AFM as a difference between top point above nucleus center and glass substrate, is 10–12 μm for NEB-1 and 9–15 μm for the KEB-7 keratin mutant cell line.

The results in Fig. 5 show that the resistance force of the immortalized control cell line NEB-1 (curve 2) is 90–170 nN for 30% deformation and 1.4–2.8 μN for 80% deformation, which is 2–3 times less than the force required for similar deformations in normal (non-immortalized) cultured human keratinocytes (see also Table 1, row 6). This difference of the compression forces between primary cultured keratinocytes (Fig. 5, curve 1) and immortalized NEB-1 keratinocytes (Fig. 5 curve 2) is likely caused by the HPV16 E6/E7 immortalization, which results in a decrease of overall keratin expression. It is been shown [41] that the immortalization by HPV16 induces the transition of differentiated epithelial cells to the less differentiated mesenchymal type of cells and leads to reduced expression of several types of cytokeratins in keratinocytes. It is also known that endogenous keratin 14 is expressed at a lower level in the HaCaT cells, another immortalized cell line, compared with primary keratinocytes and that introduction of the mutated K14 into these immortalized cells results in grossly evident filament network collapse [42]. Therefore the softness of NEB-1 cells is most likely attributed to the decreased expression level of keratins resulting in a less-dense keratin network at the perinuclear site in NEB-1 cells.

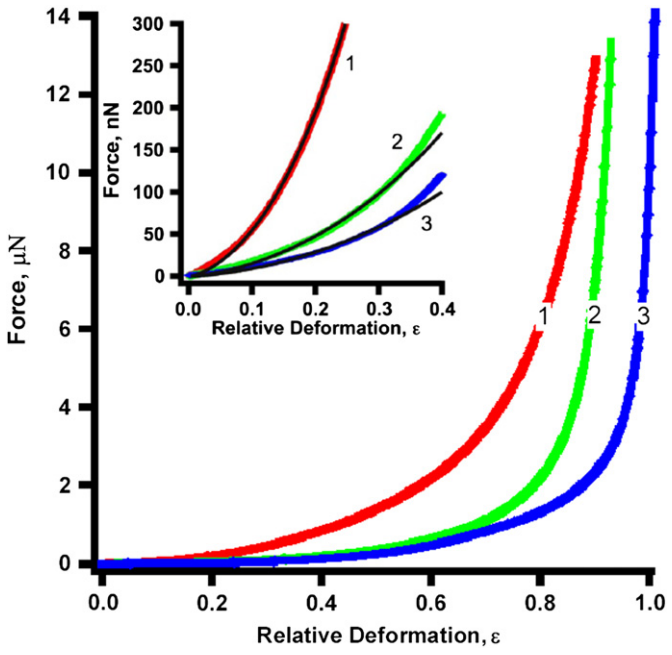

Fig. 5. Characteristic force versus relative deformation profiles for typical keratinocyte cell from primary culture (red, curve 1), NEB-1 cell line (green, curve 2) and KEB-7 cell line (blue, curve 3). Inset shows the data and least square fitting using Eq. (1) at small deformation region. (For interpretation of the references to colour in this figure legend, the reader is referred to the web version of this article).

Representative cells from keratin-mutant cell line KEB-7 (Fig. 5, curve 3) require a force of 30–90 nN to reach 30% deformation and 1–1.6 μN for 80% compression, which is 1.6–2.2 times less than that for the immortalized control NEB-1 and 4.2–6.7 times less than that for the primary keratinocytes (see also Table 1 row 7). Another remarkable fact evident from the force profile is that it requires just 4–5 μN force to compress keratin-mutant cells to almost 100% (and completely disintegrate them), while control cells rarely show deformation higher than 90% even when force as high as 50 μN is applied.

Since the only difference between KEB-7 and NEB-1 cells is the expression of the mutated K14, we conclude that keratin intermediate filaments are the critical elements playing the major role in keratinocyte mechanical resistance. This result is in good agreement with force profiles of keratinocytes with disruptured microtubules and F-actin as discussed above.

4. Conclusions

Using single cell compression, the whole-cell's mechanical response of human keratinocytes has been investigated and compared with other cell types: neuronal, prostate, breast cancer epithelial [23] and Jurkat T cells [16]. Three findings are reported, which are unique and characteristic of keratinocytes. First, the cells exhibit strong and reversible force-deformation profiles: keratinocytes are 6–70 times stiffer than the cell types mentioned above. The high mechanic strength is also manifest in the fact that a second compression cycle reveals only small softening despite the disruption of cellular membrane and subsequent cell death. Second, while Young's modulus of the keratinocyte plasma membrane is comparable with that of other cell types, the keratinocyte cytoskeleton Young's modulus range is 120–330 kPa, which is 40–60 times greater than that of Jurkat T cells. To put this result in context, such high elastic compliance is more comparable with fixed T-cells, where cytoskeletal proteins are highly crosslinked by -CONH- bonds [16]. This high elasticity is only 2–4 times smaller than Young's modulus of macroscopic human skin [33], which ranges from 420 to 850 kPa. Such close correspondence of values highlights the contribution of the keratinocyte cytoskeleton to overall skin mechanical resistance. Third, the strong single cell mechanics is attributed to keratin cytoskeletal network. This network helps the cell recover to its original shape even after cell death. We hope this investigation provided fundamental insight to bridge cellular mechanics to the protection function of our outer skin layer (epidermis).

Acknowledgements

We thank Dr. A. Mogilner for his critical review of the manuscript and advice regarding this work. Dr. J. Koehne and Dr. C. Koehler, and Ms. S. Stagner are gratefully acknowledged for their assistance in manuscript preparation. Dr. I. Leigh kindly provided the KEB-7 and NEB-1 cell lines. This work was supported by the University of California, Cancer Research Coordinating Committee, National Science Foundation (DMR0421521 and DMR0723118), and National Institute of Health (R21GM77850-01 and R01AR44518).

References

[1] T.T. Sun, C. Shih, H. Green, Proceedings of the National Academy of Sciences of the United States of America 76 (1979) 2813–2817.
[2] E. Fuchs, Annual Review of Cell and Developmental Biology 11 (1995) 123–153.
[3] D. DePianto, P.A. Coulombe., Experimental Cell Research 301 (2004) 68–76.
[4] E. Fuchs, Journal of Dermatological Science 13 (1996) 181–192.

[5] E. Fuchs, D.W. Cleveland, Science 279 (1998) 514–519.
[6] A. Hovnanian, E. Pollack, L. Hilal, A. Rochat, C. Prost, Y. Barrandon, M. Goossens., Nature Genetics 3 (1993) 327–332.
[7] Y.M. Chan, Q.C. Yu, J.D. Fine, E. Fuchs, Proceedings of the National Academy of Sciences of the United States of America 90 (1993) 7414–7418.
[8] S.M. Morley, M. D'Alessandro, C. Sexton, E.L. Rugg, H. Navsaria, C.S. Shemanko, M. Huber, D. Hohl, A.I. Heagerty, I.M. Leigh, E.B. Lane., British Journal of Dermatology 149 (2003) 46–58.
[9] T.Y. Cao, M.A. Longley, X.J. Wang, D.R. Roop., Journal of Cell Biology 152 (2001) 651–656.
[10] C. Lloyd, Q.C. Yu, J.A. Cheng, K. Turksen, L. Degenstein, E. Hutton, E. Fuchs., Journal of Cell Biology 129 (1995) 1329–1344.
[11] M.J. Arin, D.R. Roop., Cells Tissues Organs 177 (2004) 160–168.
[12] B. Peters, J. Kirfel, H. Bussow, M. Vidal, T.M. Magin., Molecular Biology of the Cell 12 (2001) 1775–1789.
[13] D.S. Fudge, K.H. Gardner, V.T. Forsyth, C. Riekel, J.M. Gosline., Biophysical Journal 85 (2003) 2015–2027.
[14] L.L. Ma, J.Y. Xu, P.A. Coulombe, D. Wirtz., Journal of Biological Chemistry 274 (1999) 19145–19151.
[15] P. Wong, P.A. Coulombe., Journal of Cell Biology 163 (2003) 327–337.
[16] V. Lulevich, T. Zink, H.Y. Chen, F.T. Liu, G.Y. Liu., Langmuir 22 (2006) 8151–8155.
[17] S. Suresh., Acta Biometerialia 3 (2007) 413–438.
[18] B.D. Hoffman, G. Massiera, K.M. Van Citters, J.C. Crocker, Proceedings of the National Academy of Sciences of the United States of America 103 (2006) 10259–10264.
[19] R.R. Isseroff, V.A. Ziboh, R.S. Chapkin, D.T. Martinez., Journal of Lipid Research 28 (1987) 1342–1349.
[20] C.E. Pullar, J.C. Grahn, W. Liu, R.R. Isseroff., Faseb Journal 20 (2006) 76–86.
[21] C.E. Pullar, A. Rizzo, R.R. Isseroff., Journal of Biological Chemistry 281 (2006) 21225–21235.
[22] S.P. Wheatley, Y.L. Wang, Indirect immunofluorescence microscopy in cultured cells, Methods in Cell Biology 57 (1998) 313–332.
[23] V. Lulevich, Y.P. Shih, S.H. Lo, G.Y. Liu., Journal of Physical Chemistry B 113 (2009) 6511–6519.
[24] D.A. Walters, J.P. Cleveland, N.H. Thomson, P.K. Hansma, M.A. Wendman, G. Gurley, V. Elings., Review of Scientific Instruments 67 (1996) 3583–3590.
[25] H.J. Butt, M. Jaschke, Nanotechnology 6 (1995) 1–7.
[26] V.V. Lulevich, O.I. Vinogradova., Langmuir 20 (2004) 2874.
[27] T.T. Sun, H. Green, Cell 9 (1976) 511–521.
[28] G.T. Charras, C.K. Hu, M. Coughlin, T.J. Mitchison., Journal of Cell Biology 175 (2006) 477–490.
[29] G.T. Charras, J.C. Yarrow, M.A. Horton, L. Mahadevan, T.J. Mitchison, Nature 435 (2005) 365–369.
[30] G. Karp, in: Cell and Molecular Biology, John Willey & Sons Inc, 2003.
[31] L. D. Landau, E. M. Lifshits, Theory of Elasticity, 3rd ed., 1965.
[32] K.N. Dahl, A.J. Engler, J.D. Pajerowski, D.E. Discher., Biophysical Journal 89 (2005) 2855–2864.
[33] P.G. Agache, C. Monneur, J.L. Leveque, J. Derigal., Archives of Dermatological Research 269 (1980) 221–232.
[34] V. Lulevich, C. Zimmer, H.S. Hong, L.W. Jin, G.Y. Liu, Proceedings of the National Academy of Sciences of the United States of America submitted (2010).
[35] Y. Tseng, T.P. Kole, J.S.H. Lee, E. Fedorov, S.C. Alino, B.W. Schafer, D. Wirtz., Biochemical and Biophysical Research Communications 334 (2005) 183–192.
[36] M. Coue, S.L. Brenner, I. Spector, E.D. Korn., Febs Letters 213 (1987) 316–318.
[37] I. Spector, N.R. Shochet, Y. Kashman, A. Groweiss, Science 219 (1983) 493–495.
[38] W.M. Morton, K.R. Ayscough, P.J. McLaughlin., Nature Cell Biology 2 (2000) 376–378.
[39] J.S. Hugon, G. Bennett, P. Pothier, Z. Ngoma., Cell and Tissue Research 248 (1987) 653–662.
[40] J. Marceiller, A. Drechou, G. Durand, F. Perez, C. Pous., Experimental Cell Research 304 (2005) 483–492.
[41] T. Geiger, H. Sabanay, N. Kravchenko-Balasha, B. Geiger, A. Levitzki, PLoS ONE 3 (2008) e1574.
[42] C.B. Sorensen, B.S. Andresen, U.B. Jensen, T.G. Jensen, P.K.A. Jensen, B. Charlotte, N. Gregersen, L. Bolund, Experimental Dermatology 12 (2003) 472–479.